01,07

Effect of crystal-chemical growth conditions of single crystals of trigonal ferroborates $Ho_{0.5}Nd_{0.5}Fe_3(BO_3)_4$ with huntite structure on their magnetic properties

© V.P. Titova, I.A. Gudim, A.V. Shabanov, E.V. Eremin ¶

Kirensky Institute of Physics, Federal Research Center KSC SB, Russian Academy of Sciences, Krasnoyarsk, Russia

¶ E-mail: eev@iph.krasn.ru

Received November 5, 2025
Revised November 19, 2025
Accepted November 20, 2025

This work aimed to compare the magnetic properties of $Ho_{0.5}Nd_{0.5}Fe_3(BO_3)_4$ single crystals grown from different solution melts: based on bismuth trimolybdate and lithium tungstate. Single crystals of this ferroborate from lithium-tungstate melt solution were grown for the first time. The chemical composition of ferroborates was determined using energy dispersive spectroscopy. It was found that Bi^{3+} ions replace Nd^{3+} ions ($\sim 5\,\%$ at.) in the case of using bismuth trimolybdate solvent. When using a lithium-tungstate melt solution, impurities from the solvent do not enter the crystal matrix. From magnetic studies, the Neel temperatures T_N and paramagnetic Curie temperatures were determined, effective magnetic moments μ_{eff} calculated, and phase diagrams of the magnetic state „temperature–magnetic field“of the studied compounds were constructed.

Keywords: solution-melt method, magnetic dielectrics, antiferromagnets.

DOI: 10.61011/PSS.2025.11.62951.311-25

1. Introduction

Rare-earth ferroborates with the structure of huntite $RFe_3(BO_3)_4$ ($R = Y$, La–Lu) attract increased attention due to their unique physical properties. These compounds have a rhombohedral structure similar to the natural mineral huntite, described by space group $R32$ or $P3_121$ The noncentrosymmetric structure makes these materials promising candidates for optical applications due to their good luminescence and nonlinear optical properties. For $RFe_3(BO_3)_4$ ferroborates it has been established that they belong to a new class of multiferroics, where magnetic, electrical, and elastic order parameters [1–7] coexist.

Magnetically, ferroborates are antiferromagnetic materials with two interacting magnetic subsystems (rare earth and iron subsystems). The iron subsystem is ordered at $T_N = 30-40$ K. The rare-earth subsystem is magnetized by the f-d interaction and essentially contributes to the magnetic anisotropy and orientation of magnetic moments. I. e. the magnetic crystallographic anisotropy is determined specifically by the type of the rare-earth ion: either an easy-axis (EA) antiferromagnetic structure is implemented, when the spins of iron ions are ordered along the trigonal c-axis ($R =$ Dy, Tb, Pr) [2], or an easy-plane (EP) structure ($R =$ Nd, Sm, Eu, Er, Y) is implemented, when the spins of iron ions are ordered in the plane ab perpendicularly to c-axis of the crystal [2]. Besides, for ferroborates $GdFe_3(BO_3)_4$ [8–10] and $HoFe_3(BO_3)_4$ [3,11], when the temperature changes, a spin-flip transition is observed from the antiferromagnetic structure with anisotropy of „easy axis“ type to the structure of „easy plane“ type. A similar transition is observed in the substituted ferroborate $Ho_{0.5}Nd_{0.5}Fe_3(BO_3)_4$ [3,12].

It is important to note that anisotropy of rare-earth ions plays a major role in the magnetoelectric properties of rare-earth ferroborates. For example, for the easy-plane ferroborates of neodymium and samarium the electrical polarization arising in magnetic fields (ΔP), had the maximum value for the ferroborates and reached $\sim 500\,\mu C/m^2$ [2]. Induced by magnetic field ΔP for ferroborates of europium and holmium ($T > 5$ K), also having easy-plane anisotropy, reaches lower, but still substantial values of around dozens $\mu C/m^2$ [3]. For highly anisotropic ions Pr^{3+}, Tb^{3+}, Dy^{3+} a magnetic structure of „easy-axis“ type is implemented, and the spins of ions Fe^{3+} are ordered below T_N along the trigonal c-axis of the crystal, which causes antiferromagnetic polarization of rare-earth ions due to f-d exchange. In this case the magnetoelectric effect has a much smaller value [2].

Initially, for isostructural nonlinear optical crystals of $RFe_3(BO_3)_4$ trigonal ferroborates, a technique was developed to grow them from melt solutions based on $K_2Mo_3O_{10}-B_2O_3$ potassium trimolybdate [13]. Later, for growing single crystals of $RAl_3(BO_3)_4$ and $RFe_3(BO_3)_4$ new melt solutions based on $Bi_2Mo_3O_{12}-B_2O_3$ bismuth trimolybdate were proposed [14]. In these melt solutions, Bi_2O_3 and MoO_3 are bound stronger than K_2O_3 and MoO_3. Therefore, the substitution of bismuth and molybdenum in the grown crystal for the rare-earth element was assumed to be relatively weak [15]. However, in some papers, the methods of chemical analysis, X-ray diffraction and magnetic studies were used to demonstrate that ions Bi^{3+} substitute the rare-earth ion in the quantity of $\sim 5-6\,\%$ at., which

nevertheless is lower than the introduction of potassium and molybdenum [16–19]. In connection with the above, the lithium tungstate-based melt-solutions were proposed. It was assumed that ions from the solvent do not enter the crystal matrix in the latter case. Indeed, paper [17] shows, using the example of ferroborate $GdFe_3(BO_3)_4$, that this is truly the case.

This paper is dedicated to the comparison of the magnetic properties of mixed ferroborates $Ho_{0.5}Nd_{0.5}Fe_3(BO_3)_4$, grown from various solvents. For this purpose a technology of growth of the substituted ferroborate $Ho_{0.5}Nd_{0.5}Fe_3(BO_3)_4$ was developed for the solution-melt on the basis of lithium tungstate $Li_2WO_4-B_2O_3$. Comparison was done to ferroborate $Ho_{0.5}Nd_{0.5}Fe_3(BO_3)_4$, grown from the solution-melt based on bismuth trimolybdate. It is important to note the special interest in this compound, since it was for it that a record value of magnetoelectric polarization was obtained in ferroborates ($\sim 900\,\mu C/m^2$) [3].

Ferroborate $Ho_{0.5}Nd_{0.5}Fe_3(BO_3)_4$ at room temperature is described by the spatial group $R32$, and at low temperatures $P3_121$ [20]. The magnetic structure is not yet known for certain. Theoretical calculations, as a possible option, suggest the presence of the angular phase below the temperature of the spin-flip transition [12].

2. Experimental techniques and sample preparation

Single crystals of ferroborate $Ho_{0.5}Nd_{0.5}Fe_3(BO_3)_4$ were grown from two solution-melt systems: based on bismuth trimolybdate $Bi_2Mo_3O_{12}-B_2O_3$, described in detail in paper [12] and on the basis of lithium tungstate $Li_2WO_4-B_2O_3$. In the last case the ferroborates $Ho_{0.5}Nd_{0.5}Fe_3(BO_3)_4$ were grown for the first time. For this purpose a technology was developed for growth from the solution-melt to a seed.

The following solution-melt was selected to grow crystals $Ho_{0.5}Nd_{0.5}Fe_3(BO_3)_4$:

80 % wt. $\{Bi_2Mo_3O_{12} + 3B2O_3 + 0.5(Nd_2O_3+Ho_2O_3)\}$ +20 % wt. $Ho_{0.5}Nd_{0.5}Fe_3(BO_3)_4$.

The following were melted to prepare 100 g of solution-melt:

B_2O_3–16.2 g, Bi_2O_3–25.6 g, MoO_3–24.0 g, Fe_2O_3–8.6 g, $Nd_2O_3-11.82$ g, $Ho_2O_3-13.78$ g.

The second solution-melt:

78 % wt. $\{Li_2WO_4 + 3.3B_2O_3 + 0.5(Nd_2O_3+Ho_2O_3)\}$ + 22 % wt. $Ho_{0.5}Nd_{0.5}Fe_3(BO_3)_4$($Li_2WO_4$–24.05 g, B_2O_3–26.62 g, Ho_2O_3–21.09 g, Nd_2O_3–18.78 g, Fe_2O_3–9.45 g).

Areas of stability of $Ho_{0.5}Nd_{0.5}Fe_3(BO_3)_4$ crystals are defined by the method of direct phase probing.

The same method was used to grow for both types of solution-melts. Solution-melts were prepared in a platinum cylindrical crucible ($D = 57$ mm, $H = 65$ mm) by subsequent fusion of oxides B_2O_3+[Bi_2O_3+MoO_3 or Li_2WO_4], [Nd_2O_3+Ho_2O_3+Fe_2O_3] at $T = 1050-1100\,^\circ$C. Then the crucible with the prepared solution-melt was placed into a crystallization furnace. The solution-melt was homogenized at $T = 1000\,^\circ$C for 5−10 h with a rod-shaped crystal holder immersed in it and rotating with the speed of $\omega = 1$ rps. The preliminary search for the saturation temperature (T_{sat}) was carried out via observations of spontaneous crystals formed on the crystal holder. After repeated homogenization T_{sat} was confirmed within $\pm 2\,^\circ$C using the crystals that were already obtained. Usually 4 „point“ seeds were fixed on the rod-shaped crystal holder, which were high quality crystals with the linear size ~ 1 mm.

The saturation temperature was 960 °C for the first and 980 °C for the second solution-melt. The width of the metastable area $\Delta T_{met} \approx 12\,^\circ$C was determined as the maximum supercooling with no spontaneous nucleation for 20 h.

After reheating of the solution-melt at $T = 1000\,^\circ$C for 2−4 h the crystal holder with the seeds was suspended above the solution-melt, and the temperature in the furnace decreased down to $T = T_{sat} + 7\,^\circ$C.

After 15 minutes the crystal holder was immersed into the solution-melt for the depth of 15−20 mm, and reversible rotation (with the period of 1 min) with the speed of $\omega = 1$ rps was activated. In $t = 15$ min. the temperature decreased down to the start $T = T_{sat} - 7\,^\circ$C, which corresponds to the middle of the metastable zone. Further the temperature of the solution-melt decreased gradually according to the program with the increasing rate 1−2 °C/day, calculated at the crystal growth speed of not more than 1 mm/day.

After the growth process was completed, the crystal holder was raised above the solution-melt and cooled down to room temperature with the furnace power supply off. The solution-melts for the 30-day cycle usually lost by evaporation not more than 2 % wt. After supplementation with the crystal-forming oxides in the quantity corresponding to the mass of the extracted crystals, they had T_{sat} close to the initial ones and were reused. The crystals were freed from the remains of the solution-melt by etching in a hot 20 % aqueous solution of nitric acid.

The magnetic properties were studied on a PPMS-9 (Quantum Design) vibration magnetometer in the in the temperature range of 4.2−300 K and magnetic fields of up to 9 T.

The chemical composition of the grown crystals was studied by the method of energy-dispersive spectroscopy (EDX) using a Bruker XFlash 430-H (Germany) detector connected to an electronic microscope. The studied crystals were attached to a metal table with the help of a two-sided conducting carbon scotch tape. Then the table with the attached samples was placed into a work chamber of a scanning electron microscope Hitachi SU3500 (Japan). To obtain the electronic microphotographs, accelerating voltage 20 kV was specified. Observation was carried out in the mode of back-scattered electrons (BSE), since in this mode the signal of reflected electrons was sensitive to the composition contrast. For each sample the parts

were selected for elemental mapping and semi-quantitative analysis of the chemical composition.

3. Experimental results

Figures 1 and 2 present the temperature dependences of magnetization of compounds $Ho_{0.5}Nd_{0.5}Fe_3(BO_3)_4$:Bi (grown from trimolybdate bismuth solution-melt) and $Ho_{0.5}Nd_{0.5}Fe_3(BO_3)_4$ (grown from tungstate lithium solution-melt) with the magnetic field orientation along (Figure 1) and perpendicularly to the triad axis of c-axis (Figure 2). From the charts you can see that at high temperatures the magnetization increases according to the Curie–Weiss law.

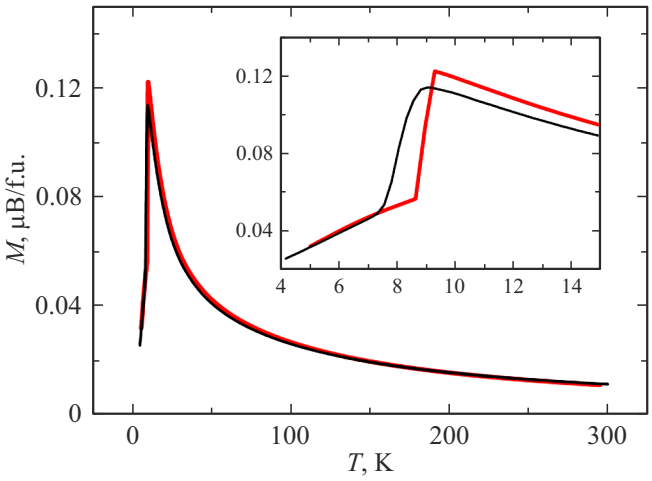

Figure 1. Temperature dependences of magnetization of compounds $Ho_{0.5}Nd_{0.5}Fe_3(BO_3)_4$:Bi (black) and $Ho_{0.5}Nd_{0.5}Fe_3(BO_3)_4$ (red), measured in the magnetic field $H = 1$ kOe, in the $H \parallel c$ geometry. The insert shows the same in a different scale.

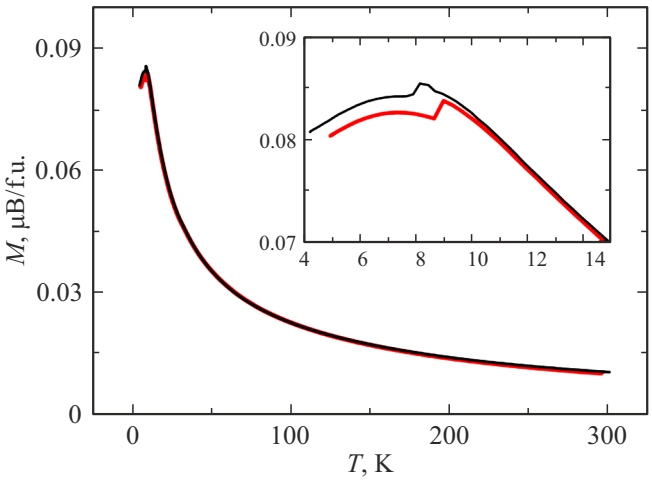

Figure 2. Temperature dependences of magnetization of compounds $Ho_{0.5}Nd_{0.5}Fe_3(BO_3)_4$:Bi (black) and $Ho_{0.5}Nd_{0.5}Fe_3(BO_3)_4$ (red), measured in the magnetic field $H = 1$ kOe, in the $H \perp c$ geometry. The insert shows the same in a different scale.

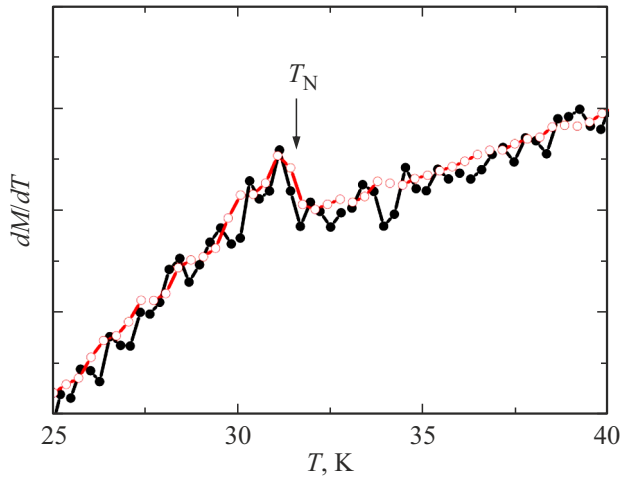

Figure 3. Temperature dependence dM/dT for $Ho_{0.5}Nd_{0.5}Fe_3(BO_3)_4$:Bi (black) and $Ho_{0.5}Nd_{0.5}Fe_3(BO_3)_4$ (red).

In the area of ~ 30 K there is a light fracture corresponding to the temperature of the antiferromagnetic ordering of the iron subsystem T_N. This transition is seen best on the derivative of the magnetization by temperature (Figure 3). You can see that Néel temperatures T_N of samples are practically the same and are equal to $T_N = 31.5$ K. This once again indicates that the long-range magnetic order in ferroborates firstly depends on the subsystem of iron ions Fe^{3+}.

Further, as the temperature decreases in the area of 8–9 K, both directions of the magnetic field $H \parallel c$ and $H \perp c$ on dependences $M(T)$ demonstrate a drastic fracture. This feature was interpreted previously as a spin-flip transition from the state of „easy plane“ (EP) type to the state of „easy axis“ (EA) type [3]. In reality the situation is much more complicated, since there might also be an angular phase in a certain temperature and magnetic field range, and also noncollinear magnetic sublattices [12]. Such transition is observed in $HoFe_3(BO_3)_4$ as well, where it is also impossible to correctly reduce the considered antiferromagnetic structure to the classic two-sublattice model.

From the dependences $M(T)$ you can see that the temperature of the spin-flip transition (T_{SR}) is approximately 1° K higher in $Ho_{0.5}Nd_{0.5}Fe_3(BO_3)_4$, then in $Ho_{0.5}Nd_{0.5}Fe_3(BO_3)_4$:Bi.

Figures 4 and 5 show the field dependences of magnetization at the various temperatures measured in the orientation of the magnetic field along and perpendicularly to the c-axis of the crystal. You can see that the spin-flip transition is observed for both magnetic field directions: $H \parallel c$ and $H \perp c$. Note that in $H \parallel c$ direction the field dependences correspond to the behavior of the two-sublattice antiferromagnetic (Figure 4). In case of magnetic field orientation perpendicularly to the c-axis of the crystal, the considered magnetic structure may not be reduced to the

collinear two-sublattice model (Figure 5). Since in case of $H \perp c$ no features must be observed, the field dependence $M(H)$ must be linear. Despite the above results, we will continue so far to interpret the observed spin-flip transition as the transition of „easy plane“ – „easy axis“ type.

From Figures 4 and 5 you can see that as the temperature increases, the critical field of the spin-flip transition (H_{SR}) moves to the area of small fields and is not observed at all above a certain temperature. Comparing $M(H)$ for this two compounds, you may note that H_{SR} for $Ho_{0.5}Nd_{0.5}Fe_3(BO_3)_4$:Bi is lower by value than H_{SR} for $Ho_{0.5}Nd_{0.5}Fe_3(BO_3)_4$ for both orientations of the magnetic field $H \parallel c$ (Figure 4) and $H \perp c$ (Figure 5).

Temperature dependences of the critical fields of transitions between the EA and EP states for both compositions and orientations of the magnetic field $H \parallel c$ and $H \perp c$ are built using $M(T)$ and $M(H)$ data. In Figure 6, where these dependences are presented, magnetic phase diagrams $Ho_{0.5}Nd_{0.5}Fe_3(BO_3)_4$:Bi and $Ho_{0.5}Nd_{0.5}Fe_3(BO_3)_4$ are shown in the corresponding magnetic fields. EA and EP states are located above and below the corresponding phase boundary.

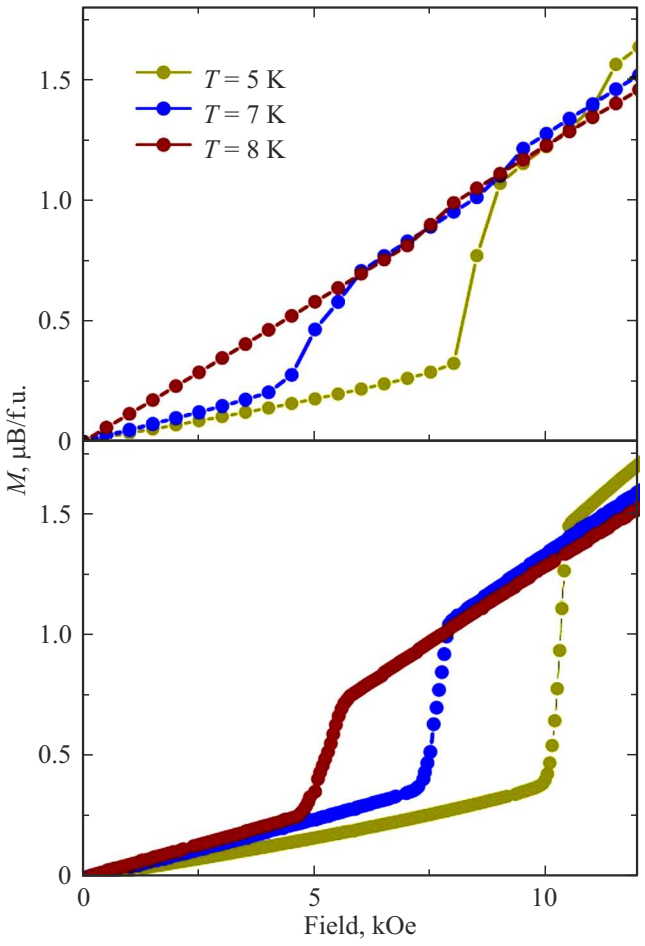

Figure 4. Field dependences of magnetization of compounds $Ho_{0.5}Nd_{0.5}Fe_3(BO_3)_4$:Bi (top) and $Ho_{0.5}Nd_{0.5}Fe_3(BO_3)_4$ (bottom), measured at different temperatures in the $H \parallel c$ geometry.

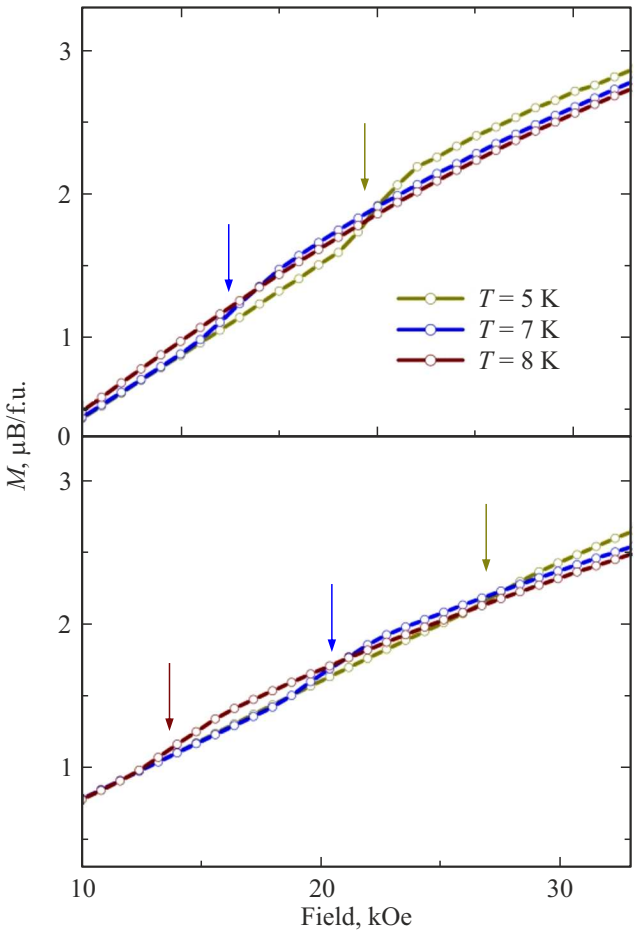

Figure 5. Field dependences of magnetization of compounds $Ho_{0.5}Nd_{0.5}Fe_3(BO_3)_4$:Bi (top) and $Ho_{0.5}Nd_{0.5}Fe_3(BO_3)_4$ (bottom), measured at different temperatures in the $H \perp c$ geometry.

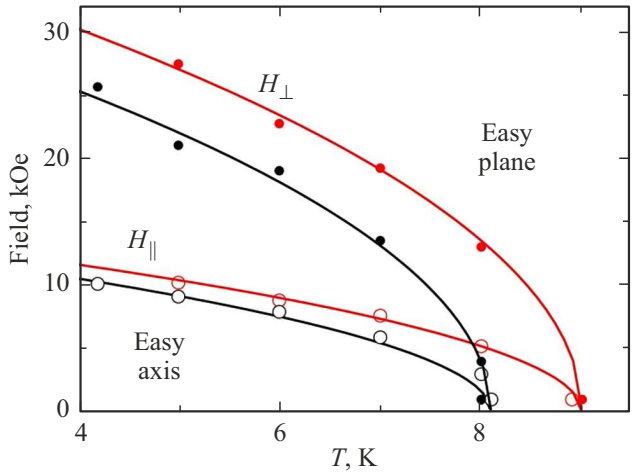

Figure 6. The magnetic phase diagram for $Ho_{0.5}Nd_{0.5}Fe_3(BO_3)_4$:Bi (black) and $Ho_{0.5}Nd_{0.5}Fe_3(BO_3)_4$ (red) in the magnetic field applied in parallel and perpendicularly to the c-axis of the crystal.

From the diagrams you can see that the value of the spin-flip transition is higher for $Ho_{0.5}Nd_{0.5}Fe_3(BO_3)_4$, than for $Ho_{0.5}Nd_{0.5}Fe_3(BO_3)_4$:Bi in the entire $(T-H)$ space.

Magnetic parameters of the studied compounds

	$Ho_{0.5}Nd_{0.5}Fe_3(BO_3)_4$:Bi	$Ho_{0.5}Nd_{0.5}Fe_3(BO_3)_4$
Confirmed composition	$Ho_{0.50}Nd_{0.45}Bi_{0.05}Fe_3(BO_3)_4$	$Ho_{0.42}Nd_{0.58}Fe_3(BO_3)_4$
T_N, K	31.5	31.5
$\theta_{\parallel}$, K	−55.1	−38.5
$\theta_{\perp}$, K	−80.4	−66.1
μ_{eff}, μ_B	13.3	12.8
μ_{theor}, μ_B	12.95	12.73

4. Discussion of results

In the paramagnetic area for both compositions the magnetization is ruled by Curie-Weiss law, where you can find the paramagnetic Curie θ temperatures and effective magnetic torque μ_{eff}. Experimentally found θ depend both on the composition and the direction of the magnetic field (see table). The negative sign θ indicates the presence of antiferromagnetic exchange interaction in the magnetic system, which is typical for all ferroborates with the huntite structure. You can see that the value θ has a lower value (by absolute value) in $Ho_{0.5}Nd_{0.5}Fe_3(BO_3)_4$, vs. $Ho_{0.5}Nd_{0.5}Fe_3(BO_3)_4$:Bi. This fact was a surprise. It seemed it had to be the other way round, since non-magnetic bismuth ions Bi^{3+} had to substitute magnetic ions Nd^{3+} and Ho^{3+}.

The experimentally determined effective magnetic torque of one structural unit μ_{eff} was calculated from the tangent of inclination of the inverse dependence of temperature dependence of magnetic susceptibility $\chi^{-1}(T)$ and is presented in the table. It turned out that the effective magnetic torque in compound $Ho_{0.5}Nd_{0.5}Fe_3(BO_3)_4$:Bi is higher by $0.5\,\mu_B$ than in $Ho_{0.5}Nd_{0.5}Fe_3(BO_3)_4$, even though it had to be the other way round here as well.

The theoretical value of the effective magnetic torque may be calculated as follows:

$$\mu_{\text{theor}} = \sqrt{3 \cdot g_S^2 \cdot \langle S_{\text{Fe}} \rangle^2 \cdot \mu_B^2 + n1 \cdot g_{J\text{Ho}}^2 \cdot \langle J_{\text{Ho}} \rangle^2 \cdot \mu_B^2 + \\ + n2 \cdot g_J\text{Nd}^2 \cdot \langle J_{\text{Nd}} \rangle^2 \cdot \mu_{\text{B}}^2}, \quad (1)$$

where $g_S = 2$ — g-factor accounting for only the spin magnetic torque, $g_{J\text{Ho}} = 5/4$ — Landé factor for ion Ho^{3+}, $g_{J\text{Nd}} = 8/11$ — Landé factor for ion Nd^{3+}, $\langle S_{\text{Fe}} \rangle^2 = S \cdot (S+1)$ — square of operator of iron ion spin moment ($S = 5/2$ for Fe^{3+}), $\langle S_{\text{Ho}} \rangle^2 = J \cdot (J+1)$ — square of operator of holmium ion full moment ($J = 8$ for Ho^{3+}), $\langle S_{\text{Nd}} \rangle^2 = J \cdot (J+1)$ — square of operator of neodymium ion full moment ($J = 8$ for Nd^{3+}), $n1$, $n2$ — share of holmium and neodymium ions, accordingly ($n1 + n2 = 1$).

If the ideal case is suggested that holmium and neodymium ions enter the crystal matrix at the ratio of 1 : 1, and there are no impurities, in this case the theoretical value of μ_{eff} will be equal to $12.95\,\mu_B$. This value is close to the experimentally defined values μ_{eff} for $Ho_{0.5}Nd_{0.5}Fe_3(BO_3)_4$ and $Ho_{0.5}Nd_{0.5}Fe_3(BO_3)_4$:Bi. However, a question arises — why μ_{eff} for $Ho_{0.5}Nd_{0.5}Fe_3(BO_3)_4$ is below the theoretical one, and for $Ho_{0.5}Nd_{0.5}Fe_3(BO_3)_4$:Bi it is higher?

Therefore, to understand a fuller picture, the EDX method was used in an attempt to define the chemical composition of the studied compounds. The compositions of both compounds were defined based on the analysis of X-ray fluorescence specta in Figure 7. Use of Quantax Espirit software suite yields the following calculation results: $Ho_{0.50}Nd_{0.45}Bi_{0.05}Fe_3(BO_3)_4$ — for the sample grown from bismuth trimolybdate solution-melt and $Ho_{0.42}Nd_{0.58}Fe_3(BO_3)_4$ — for the sample grown from lithium tungstate solution-melt. It should be noted that the relative error in the composition definition was $\delta = 1.5\,\%$.

Such different content of Ho^{3+} and Nd^{3+} ions in ferroborates may be explained as follows. As is known, when crystals are made from bismuth molybdate solution-melt, partial substitution occurs in the rare earth subsystem. Besides, taking into account the fact that the ionic radius of neodymium Nd^{3+} is closer to the ionic radius of bismuth Bi^{3+} (98.3 and 120 pm, respectively), and a substantially larger difference with the ionic radius of holmium (90 pm), substitution mostly happens in the neodymium subsystem.

For the lithium tungstate system there can be no such substitution, since ionic radii of lithium and tungsten (73 pm and 62 pm, respectively) differ substantaally from ionic radii of rare earths. Here, probably, the coefficients of distribution among the crystal and the solution-melt are slightly higher than one for neodymium and lower for holmium. In this case the distribution coefficient may not be calculated in advance, but may only be selected using experimental data.

For understanding of the entire picture of magnetic behavior, it is necessary to take into account all competing exchange interactions in this compound [12]. As it known, magnetic torques of iron ions Fe^{3+} in $HoFe_3(BO_3)_4$ are antiferromagnetically ordered at $T_N \sim 38-39\,\text{K}$, and when temperature lowers down to T_{SR}, some of them lie in the basal plane ab, as well as all magnetic torques of Ho^{3+} ions, and other Fe^{3+} ions are arranged at the angle to the plane [21]. At $T_{SR} = 4.7\,\text{K}$ the spontaneous spin-flip transition occurs, as a result of which the magnetic torques of holmium are arranged at the angle to the third order

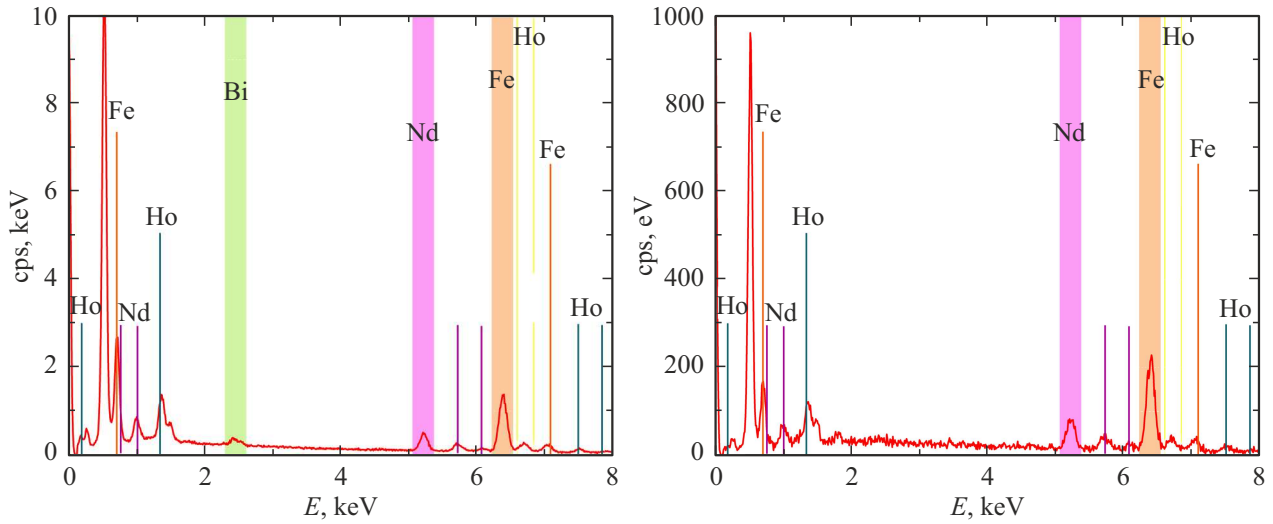

Figure 7. Spectrum of X-ray radiation from samples $Ho_{0.5}Nd_{0.5}Fe_3(BO_3)_4$, grown using bismuth trimolybdate (left) and lithium tungstate (right) solution-melts.

axis, while the Fe-subsystem becomes oriented along the c-axes. In $NdFe_3(BO_3)_4$ at $T < T_N \sim 31$ K all magnetic torques are in the basal plane ab [22]. Therefore, as a result of competition of different contributions from Ho-, Nd- and Fe-subsystems to the magnetic anisotropy, spontaneous and magnetic field inducted spin-flip transitions may arise in $Ho_{1-x}Nd_xFe_3(BO_3)_4$ compound.

Such transitions were detected for $x = 0.5$ [3,12] and 0.75 [23] compositions. It seemed evident that substitution of Ho^{3+} ions for Nd^{3+} ions that stabilized the easy plane state in $Ho_{1-x}Nd_xFe_3(BO_3)_4$ should have resulted in the temperature shift of the spin-flip transition from the EP type state to EA state from the value detected in $HoFe_3(BO_3)_4$ ($T_{SR} = 4.7$ K) to the area of lower temperatures. However, in $Ho_{0.5}Nd_{0.5}Fe_3(BO_3)_4$ temperature T_{SR} suddenly increased to 8 K [3], and in $Ho_{0.25}Nd_{0.75}Fe_3(BO_3)_4$ the value T_{SR} remained approximately the same as in $HoFe_3(BO_3)_4$ [23]. This result clearly shows that simple summation of contributions from EA- and EP-subsystems in the substituted compound is not enough to explain the processes happening in the resulting magnetic structure. Thus, paper [12] shows that increase of T_{SR} in $Ho_{0.5}Nd_{0.5}Fe_3(BO_3)_4$ (compared to $HoFe_3(BO_3)_4$) is caused by expansion of the temperature range of the initial low-temperature state of the magnetic subsystem as a result of its change from the easy axis state (as in $HoFe_3(BO_3)_4$) to the angular state.

Therefore, it is evident that the temperature of spin-flip transition in $Ho_{1-x}Nd_xFe_3(BO_3)_4$, first of all depends on holmium ion Ho^{3+}, besides, this contribution is non-linear and depends on its content in $Ho_{1-x}Nd_xFe_3(BO_3)_4$.

Figure 8 shows the dependence of temperature T_{SR}, determined in the magnetic field 1 kOe, on the content of Ho^{3+} ions in the $Ho_{1-x}Nd_xFe_3(BO_3)_4$ compound. You can see that as concentration x increases, temperature T_{SR} grows

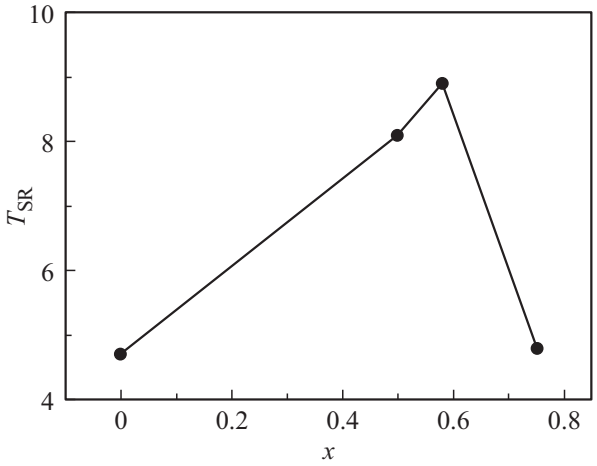

Figure 8. Dependence of temperature of spin-flip transition T_{SR} in $Ho_{1-x}Nd_xFe_3(BO_3)_4$ on concentration x. The data for $x = 0$ is taken from paper [11], for $x = 0.75$ from paper [23], others—from the presented paper.

first, reaches its maximum in the range of $x = 0.58-0.75$, and only after the maximum value is achieved, it starts decreasing.

However, it should be noted that you should not reduce everything to the impact of Ho^{3+} ions. In paper [12] within the single theoretical approach based on the approximation of the molecular field and calculations in the model of the crystalline field for a rare-earth ion it was shown that this spin-flip transition is caused by various temperature dependences of the competing contributions of rare-earth (Ho and Nd) and Fe-subsystems to the full magnetic anisotropy $Ho_{1-x}Nd_xFe_3(BO_3)_4$. Therefore, for more complete understanding of the observed magnetic behavior it is further necessary to additionally study the diffraction of neutron elastic scattering.

5. Conclusion

For the first time $Ho_{1-x}Nd_xFe_3(BO_3)_4$ single crystals were grown from the lithium tungstate solution-melt (with $x = 0.5$ for charging). For the purpose of comparison, $Ho_{1-x}Nd_xFe_3(BO_3)_4$ single crystals ($x = 0.5$ for charging) were grown with the use of a solvent based on bismuth trimolybdate. A comparative analysis of magnetic properties of the grown ferroborates was carried out.

The EDX method was used to determine the chemical composition of ferroboratea: $Ho_{0.50}Nd_{0.45}Bi_{0.05}Fe_3(BO_3)_4$ — for the sample grown from bismuth trimolybdate solution-melt and $Ho_{0.42}Nd_{0.58}Fe_3(BO_3)_4$ — for the sample grown from lithium tungstate solution-melt. It was shown that Bi^{3+} ions mostly substitute neodymium ions Nd^{3+}, if the growth is carried out from the bismuth trimolybdate solution-melt. In case of use of lithium tungstate solvent, neither lithium ions, nor tungsten ions enter the crystal matrix. However, it turned out that the coefficients of distribution among the crystal and the solution-melt are slightly higher than one for neodymium and lower for holmium. It is related to the fact that the distribution coefficient may not be calculated in advance, but may only be selected using experimental data.

The magnetic studies identified the Néel temperatures, paramagnetic Curie temperatures, effective magnetic torques μ_{eff} were calculated. In both cases μ_{eff} turned out to be slightly higher than the one calculated theoretically, with account of the chemical composition for these compounds. „Temperature–magnetic field" phase diagrams of the magnetic state for the crystals under study are plotted.

It was shown that the shift of the spin-flip transition T_{SR} in $Ho_{0.42}Nd_{0.58}Fe_3(BO_3)_4$ in the area of higher temperatures and fields, compared to $Ho_{0.50}Nd_{0.45}Bi_{0.05}Fe_3(BO_3)_4$ complies with the representation that the concentration of Ho^{3+} ions in $Ho_{1-x}Nd_xFe_3(BO_3)_4$ impacts non-linearly by the value T_{SR} with a pronounced maximum in the range of $x = 0.58-0.75$. For complete understanding of magnetic behavior further research of neutron elastic scattering diffraction is necessary.

Acknowledgments

The authors thank the Krasnoyarsk Regional Research Equipment Sharing Center of the Federal Research Center (FRC) Krasnoyarsk Science Center (KSC) of the Siberian Branch (SB) of the Russian Academy of Sciences (RAS) for the provided equipment.

Funding

The study was carried out within the range of research topics under the state assignment of the Kirensky Institute of Physics, SB RAS.

Conflict of interest

The authors declare that they have no conflict of interest.

References

[1] A.K. Zvezdin, S.S. Krotov, A.M. Kadomtseva, G.P. Vorob'ev, Yu.F. Popov, A.P. Pyatakov, L.N. Bezmaternykh, E.A. Popova, Pisma v ZhETF **81**, *6*, 335 (2005). (in Russian).
[2] A.M. Kadomtseva, Yu.F. Popov, G.P. Vorob'ev, A.P. Pyatakov, S.S. Krotov, K.I. Kamilov, V.Yu. Ivanov, A.A. Mukhin, A.K. Zvezdin, A.M. Kuz'menko, L.N. Bezmaternykh, I.A. Gudim, V.L. Temerov. FNT **36**, *6*, 640 (2010). (in Russian).
[3] R.P. Chaudhury, F. Yen, B. Lorenz, Y.Y. Sun, L.N. Bezmaternykh, V.L. Temerov, C.W. Chu. Phys. Rev. B **80**, *10*, 104424 (2009).
[4] A.N. Vasiliev, E.A. Popova, FNT **32**, *8/9*, 968 (2006). (in Russian).
[5] V.I. Zinenko, M.S. Pavlovskiy, A.S. Krylov, I.A. Gudim, E.V. Eremin, ZhETF **144**, *6*, 1174 (2013). (in Russian).
[6] A.P. Pyatakov, A.K. Zvezdin, UFN **182**, *6*, 593(2012). (in Russian).
[7] T. Usui, Y. Tanaka, H. Nakajima, M. Taguchi, A. Chainani, M. Oura, S. Shin, N. Katayama, H. Sawa, Y. Wakabayashi, T. Kimura. Nat. Mater. **13**, *6*, 618 (2014).
[8] A.I. Pankrats, G.A. Petrakovsky, L.N. Bezmaternykh, O.A. Bayukov, ZhETF **246**, *10*, 887 (2004). (in Russian).
[9] A.D. Balaev, L.N. Bezmaternykh, I.A. Gudim, V.L. Temerov, S.G. Ovchinnikov, S.A. Kharlamova. JMMM **258–259**, 532 (2003).
[10] H. Mo, C.S. Nelson, L.N. Bezmaternykh, V.L. Temerov. Phys. Rev. B **78**, 214407 (2008).
[11] A. Pankrats, G. Petrakovskii, A. Kartashev, E. Eremin, V. Temerov. J. Phys.: Condens. Matter **21**, 436001 (2009).
[12] I.A. Gudim, A.A. Demidov, E.V. Eremin, D.K. Shukla. FTT **60**, *10*, 1947 (2018). (in Russian).
[13] N.I. Leonyuk, L.I. Leonyuk. Prog. Cryst. Growth Ch. **31**, 179 (1995).
[14] L.N. Bezmaternykh, V.L. Temerov, I.A. Gudim, N.A. Stolbovaya. Cryst. Rep. **50**, 97 (2005).
[15] K.N. Boldyrev, M.N. Popova, M. Bettinelli, V.L. Temerov, I.A. Gudim, L.N. Bezmaternykh, P. Loiseau, G. Aka, N.I. Leonyuk. Optic. Mat. **34**, *11*, 1885 (2012).
[16] I.S. Lyubutin, A.G. Gavriliuk, N.D. Andryushin, M.S. Pavlovskiy, V.I. Zinenko, M.V. Lyubutina, I.A. Troyan, E.S. Smirnova. Cryst. Growth Des. **19**, *12*, 6935 (2019).
[17] I.A. Gudim, E.V. Eremin, N.V. Mikhashenok, V.R. Titova. FTT **65**, (in Russian). *2*, 243 (2023).
[18] E.V. Eremin, I.A. Gudim, V.R. Titova. FTT **65**, *11*, 1925 (2023). (in Russian).
[19] I.A. Gudim, V.R. Titova, E.M. Moshkina, M.S. Pavlovsky, A.S. Krylov, E.V. Eremin. FTT **66**, *11*, 1986 (2024). (in Russian).
[20] A. Tripathy, K. Gautam, K. Dey, S.R. Sahu, A. Ahad, A. Upadhyay, A. Sagdeo, S. Francoual, P.J. Bereciartua, I. Gudim, J. Strempfer, V.G. Sathe, D.K. Shukla. Phys. Rev. B **107**, 214106 (2023).
[21] C. Ritter, A. Vorotynov, A. Pankrats, G. Petrakovskiĭ, V. Temerov, I. Gudim, R. Szymczak. J. Phys.: Condens. Matter **20**, 365209 (2008).
[22] M. Janoschek, P. Fischer, J. Schefer, B. Roessli, and V. Pomjakushin, M. Meven, V. Petricek, G. Petrakovskii, L. Bezmaternikh. Phys. Rev. B **81**, 094429 (2010).
[23] R.P. Chaudhury, B. Lorenz, Y.Y. Sun, L.N. Bezmaternykh, V.L. Temerov, C.W. Chu. J. Appl. Phys. **107**, 09D913 (2010).

Translated by M.Verenikina